DOI: 10.1002/chem.200700569

Proton Activity Inside the Channels of Zeolite L

Rodrigo Q. Albuquerque and Gion Calzaferri*[a]

Abstract: The proton activity inside the channels of zeolite L has been studied by investigating dye-loaded zeolite L crystals under different conditions, such as water content, nature of the counterions, and nature of the solvent. The discussion is made within the frame of three types of dye-loaded zeolite L systems, classified according to their ability to exchange matter (dyes, cations, solvent, and other small molecules) with the environment. The classification refers to dye-loaded zeolites. The term "closed" and "semi-open" characterize different possibilities of the channels to exchange small molecules, cations, and solvent molecules with the environment, but not dyes. The "open" systems also allow for dye exchange. UV-visible and fluorescence spectroscopy have been used to observe the proton activity inside the zeolite L channels. The influence of the proton activity on the luminescence of encapsulated dyes is discussed, special attention being given to luminescence quenching by excited-state protonation. Partially proton-exchanged zeolite L can be a superacid, whereas for the M-exchanged form (M: K^+, Li^+, Cs^+, Mg^{2+}, Ca^{2+}) the pH ranges from about 2.5 to 3.5. For these last forms, the differences in pH are due to the acid–base reactions of the respective metal cations with water inside the zeolite. Finally, we describe an easy experimental procedure that can be used to tune the proton activity inside the zeolite L to a considerable extent.

Keywords: dyes/pigments · host–guest systems · luminescence · supramolecular chemistry · zeolites

Introduction

Zeolites play an important role in petrochemical processes, in which they act as size-selective catalysts in cracking reactions.[1] The efficiency in catalyzing these reactions stems from their high acidity, which is mainly due to the presence of Brønsted sites. The acid sites are formed after calcination of the zeolite as the protonated H-form is produced. Classical zeolites are built up by corner-sharing TO_4 tetrahedra (T: Si, Al) forming a three-dimensional system of channels and cavities. The substitution of a tetravalent silicon atom by a trivalent aluminum atom in a TO_4 unit generates a negative charge, which is then balanced by a charge-compensating cation. These cations can be completely or partially replaced by means of ion exchange, depending on the type of zeolite, giving rise to a large variety of cation-exchanged zeolites. Hydrolysis and calcination leads to the formation of Brønsted sites as explained in Scheme 1, which shows a simplified view of a zeolite represented by two TO_4 units and Na^+, H_3O^+, and NH_4^+ as counterions. Brønsted sites are produced by hydrolysis (reaction I), followed by calcination (reaction II).[2]

Reaction I explains why suspensions of exchanged zeolite crystals in distilled water tend to be basic, whereas at the same time the proton concentration and, therefore, the acidity inside the cavity increases. For example, calcination of zeolite ZSM-5 at 400 °C leads to the highest acidity due to the formation of Brønsted sites, whereas calcination at 700 °C leads to fully hydrated predominance of Lewis acid sites.[3]

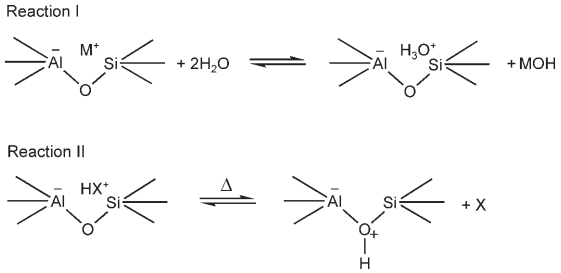

Scheme 1. Schematic representation of a zeolite showing the formation of Brønsted sites through hydrolysis (I) and calcination (II). M^+ is a charge compensating cation and X: H_2O, NH_3, $NH(CH_3)_2$, or other small molecules.

[a] Dr. R. Q. Albuquerque, Prof. Dr. G. Calzaferri
Department of Chemistry and Biochemistry
University of Bern, Freiestrasse 3, 3012 Bern (Switzerland)
Fax: (+41) 316313994
E-mail: gion.calzaferri@iac.unibe.ch

The acidic proton shown in Scheme 1 is usually bonded to one of the four oxygen atoms surrounding the negatively charged aluminum. It can jump from one oxygen to another and its mobility is greatly increased in the presence of H_2O or by heating.[4] Several methods have been used to study the Brønsted acidity, such as microcalorimetry,[5] solid-state NMR spectroscopy,[6] temperature-programmed desorption,[7] vibrational and electronic spectroscopy,[8–10] and quantum mechanical calculations.[11]

Brønsted sites influence the photophysical behavior of dyes encapsulated into zeolite L crystals and, therefore, they can affect the properties of photonic antenna systems based on dye–zeolite host–guest materials. The luminescence of the dyes as a rule is increased upon encapsulation, because of space restrictions inside the small one-dimensional (1D) channels, which do not allow large-amplitude motions and also suppress luminescence quenching caused by bimolecular reactions or aggregate formation.[12] The acidity of the Brønsted sites can, however, influence the luminescence of encapsulated dyes by means of ground- or excited-state protonation to a considerable extent. For example, a strong luminescence quenching of Hostasol Red (see Scheme 2) is observed as a result of fast nonradiative deactivation paths due to excited-state protonation. Another example is oxonine, which is highly fluorescent in the monoprotonated form and nonfluorescent in the diprotonated form.[13] Zeolite L can be made so acidic that degradation of acid-labile dyes can occur. Therefore, understanding and controlling the proton activity inside the channels is important if one wishes to achieve optimal photophysical properties of dye-loaded zeolite L, host–guest materials.

The photophysical behavior of encapsulated dyes is influenced not only by protons, but also by interactions with other counterions present in the zeolite. These interactions depend on the presence or absence of solvent molecules, such as toluene, methanol, or water. Encapsulated dyes are usually adsorbed on the walls of the main channel, where many cations are located. In the absence of a solvent, a direct interaction between dyes and cations takes place and, as a consequence, changes observed in the spectra are strongly correlated with the nature of the counterions. Under this condition, the heavy-atom effect can play an important role.[14] Increasing the content of solvent molecules inside the zeolite leads to solvation of the counterions, which then weakens their interaction with the dyes. In this case, the interaction between the dyes and the protons becomes more important than the nature of the counterion. This is the situation we are mainly addressing here. The stoichiometry of zeolite L with monovalent cations M that contains some protons is $M_{9-x}H^+_x(SiO_2)_{27}(AlO_2)_9{\cdot}n\,H_2O$ in which $n=21$ in fully hydrated materials.[12] This means that the number of water molecules in an acid–base reaction of dye molecules D located inside the zeolite L channels, Equation (1), can not be considered as being constant. This is expressed in Equation (2), in which K_a is the acidity constant expressed by means of the activities a of the corresponding species.

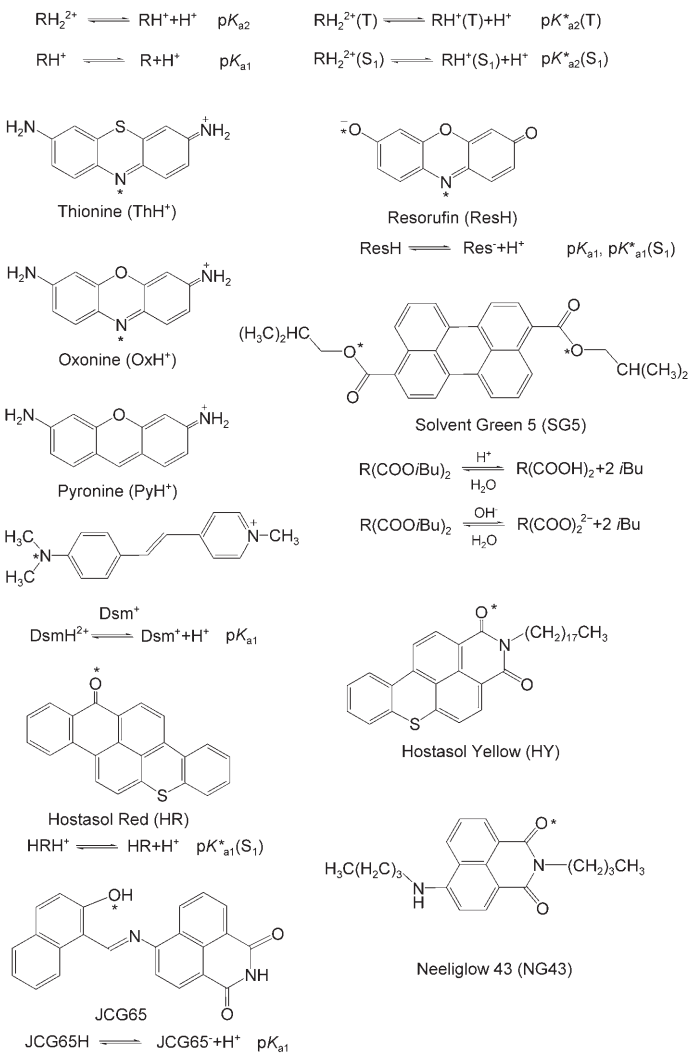

Scheme 2. Top: Equilibrium equations. R: dye; S_1: singlet excited state; T: triplet state; $pK_a^*(X)$ corresponds to the pK_a in the X excited state (X: T or S_1). Bottom: Structure of organic dyes. The * shown in the structures indicate at which position protonation can occur. The abbreviations used for the dyes are slightly different from those often found in the literature in order to emphasize their protonated states. Ground- and excited-state pK_a values measured in H_2O (thionine, oxonine, Dsm^+, and Resorufin) and in DMSO (JCG65 and Hostasol Red). Thionine (ThH^+): $pK_{a1}=11.0$,[22] $pK_{a2}=-0.33$,[23] $pK^*_{a2}(S_1)=3.1$, $pK^*_{a2}(T)=6.3$;[23] oxonine (OxH^+): $pK_{a2}=-1.2$, $pK_{a1}=11.27$,[24,25] $pK^*_{a2}(S_1)=1.2$;[25] Dsm^+: $pK_{a1}=3.7$[26]; Hostasol Red (HR): $pK^*_{a1}(S_1)=1$–2; JCG65: $pK_{a1}=8$–9; Resorufin (ResH): $pK_{a1}=5.5$,[27] $pK^*_{a1}(S_1)=-1.3$[28]; For Pyronine the second protonation, which occurs at the carbon atom, breaks the long π system of the dye and causes PyH^{2+} solutions to be colorless.

$$D + H_3O^+ \rightleftharpoons DH^+ + H_2O \quad (1)$$

$$K_a = \frac{a_{DH^+}}{a_D}\frac{a_{H_2O}}{a_{H_3O^+}} \quad (2)$$

Solving Equation (2) for the proton activity and expressing the result in terms of concentrations and activity coefficients γ, we obtain Equation (3).

$$a_{H_3O^+} = \frac{[DH^+]}{[D]}\frac{[H_2O]}{K_a}\frac{\gamma_{DH^+}\gamma_{H_2O}}{\gamma_D} \quad (3)$$

This means that the proton activity inside the zeolite channels can be obtained by measuring the ratio $[DH^+]/[D]$ by means of electronic absorption spectroscopy. The change of the number of water molecules in the protonation reaction in Equation (1) can be taken into account. It is not so important for fully hydrated zeolite, but can become very important in partially hydrated materials. It would be desirable to have more quantitative information about the activity coefficient term, which will not be addressed here. It is, however, useful to keep in mind that the $[H_3O^+]/[H_2O]$ ratio of a fully hydrated zeolite L containing one proton per unit cell is about 0.047. This corresponds to the acidity of a 2.5 M hydrochloric acid solution.[9]

This work aims at investigating the proton activity inside the channels of zeolite L and to understand its influence on the photophysical properties of encapsulated dyes. The discussed concepts are also valid for other microporous and mesoporous systems.

Materials and Methods

Zeolite L: Zeolite L is an aluminosilicate composed of thousands of parallel channels featuring hexagonal symmetry (see Figure 1). The fully hydrated crystal has stoichiometry

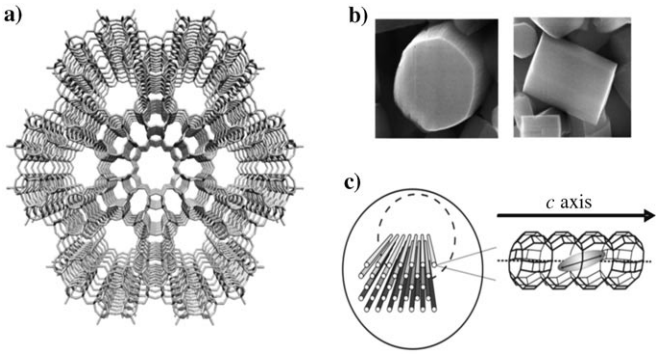

Figure 1. a) Structure of a zeolite L crystal viewed from the top (the counterions are omitted for clarity); b) SEM pictures of two crystals of about 2 μm length and 1.5 μm diameter showing the base and coat of zeolite L crystals; c) Pictorial view of the parallel 1D channels of zeolite L. The zoom on the right shows a main channel with an encapsulated dye with the transition dipole moment oriented as indicated by the double arrow.

$M_9(SiO_2)_{27}(AlO_2)_9{\cdot}21\,H_2O$, in which M is a monovalent charge-compensating cation, necessary because the zeolite L framework is negatively charged. Out of the nine cations per unit cell, 3.6 are located in the large channel and can be exchanged without loss of crystallinity. A large number of different luminescent organic dyes can be easily inserted into the main channels of zeolite L, the openings of which have a Van der Waals diameter of 7.1 Å.[15] This is done in the gas phase for neutral dyes, or in solution by means of ion exchange for cationic dyes. A very high dye concentration in the monomeric form can be achieved by this encapsulation. Förster energy transfer between the encapsulated dyes has been observed to be very fast and efficient[16] and has been used to establish communication between the inside of dye-loaded zeolite L crystals and an acceptor located at a specific place on the outer surface of the crystals.[17]

Dye-loaded zeolite L crystals can be functionalized with the so-called stopcock molecules.[12,17–19] These molecules have a tail that penetrates into the channels and a head which is too bulky to enter (Figure 2).

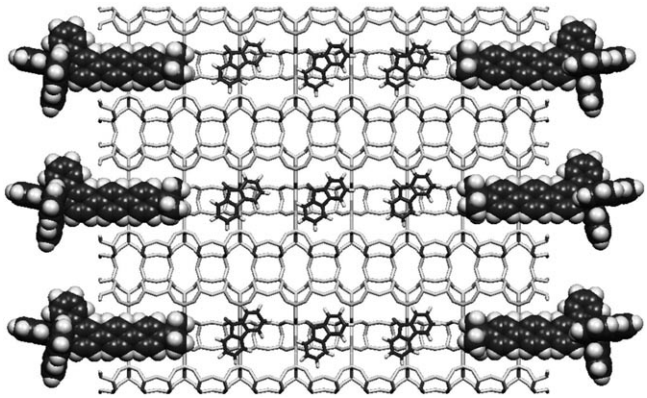

Figure 2. Pictorial view of a section of a dye-loaded zeolite L crystal functionalized with the so-called stopcock molecules, which close the channel entrances.

The stopcocks allow communication between the encapsulated dyes and the chemical environment outside the zeolite L, for example, by means of fluorescence resonance energy transfer, FRET.[19] The zeolite L crystals can be further organized to form an oriented monolayer, in which the crystals are aligned with the *c* axis perpendicular to a substrate, to which they are covalently bonded.[17,20] Therefore, a highly anisotropic material can be built, which is very important in the design of monodirectional photonic antennae.[17,21]

Dyes: The dyes discussed in this work are shown in Scheme 2, together with some pK_a values of the ground and excited states. In this work, the dye concentration inside the zeolite L has been expressed in terms of the loading, which varies from 0 to 1. A loading of 0.5, for example, indicates that 50% of the available zeolite sites are occupied by dyes.[12]

Methods: The Brønsted acidity of dye-loaded zeolite L crystals was investigated through the analysis of the fluorescence and absorption spectra of dyes in solution and encapsulated dyes, both under different conditions (pH of the solution, water content, nature of the zeolite counterion, and nature of the solvent). Molecular orbital calculations were carried out to help with the interpretation of the experiments.

Results

The investigated systems have been shown to be heterogeneous in nature, because the encapsulated dyes can be influenced by cations, by the solvent, and by other molecules present inside the channels or cavities. For this reason, the systems have been divided into three main types (shown in Table 1) that have been grouped according to their ability to exchange matter with the environment. The definitions refer to dye-loaded zeolites. The term "closed" and "semi-open" characterize different possibilities of the channels to exchange small molecules, cations, and solvent molecules with the environment, but not dyes. The "open" systems also allow for dye exchange. Whether the conditions are satisfied depends, in general, not only on the nature of the channel entrances and on the dyes, but also on the nature of the environment. It is very important to have full control of the external surface of the crystals when synthesizing dye-loaded zeolite L materials. Washing the crystals with an appropriate solvent is the most successful method to eliminate unwanted molecules from the outer surface. Knowledge of the category to which a system belongs is also important for this purpose.

Table 1. System types describing the ability of dye–zeolite crystals to exchange matter with the environment (Y = yes).

Matter exchanged	System type						
	closed	semi-open				open	
		I	II	III	IV	I	II
dyes	–	–	–	–	–	Y	Y
small molecules (not solvent; e.g. O_2, N_2)	–	Y	Y	Y	Y	Y	Y
small cations (e.g., H^+, Na^+, Ca^{2+})	–	–	–	Y	Y	–	Y
solvent	–	–	Y	–	Y	Y	Y

Examples of the system types given in Table 1 are described as follows.

Closed: Dye-loaded zeolite L crystals with channel entrances plugged by means of stopcock molecules that do not allow any molecules or ions to pass is the typical example. Dye-loaded zeolite L crystals in a flame-sealed evacuated ampoule also characterizes a closed system.

Semi-open I: The stopcock may be such that small molecules can pass, but not the dyes. This situation may also be realized in the absence of stopcocks if, for example, zeolite L crystals loaded with cationic dyes are suspended in solvents composed of relatively bulky nonpolar molecules, which do not allow cation or dye exchange because the solvent has no ability to accept charged species.

Semi-open II: Systems of this type are very similar to those of the semi-open I type, the only difference being that now the nonpolar solvent is composed of small molecules that can pass through the space left between the dye and the zeolite framework.

Semi-open III: Only exchange with small cations such as protons, alkali, or alkaline-earth metals and similar ions can occur, whereas the used solvent molecules cannot enter for steric reasons. This is achieved when dye-loaded zeolite L crystals are suspended in a polar solvent, the molecules of which are too big to enter the channels that might be partially blocked by means of stopcocks.

Semi-open IV: This can be achieved by plugging the channels with specific stopcocks, by encapsulating dyes with a strong interaction with the zeolite channels, or if the encapsulated dyes are polymerized.

Open: This system always allows dye exchange, insofar as the dye has the appropriate size to pass through the channel openings. In this work we present many situations in which the systems can be described by the open II type, in which all species can be exchanged. The open I type can, however, be also observed, if cation-exchanged zeolite L loaded with neutral dyes is suspended in a solvent composed of small nonpolar molecules in which the dye is soluble. A typical example of such system is given by K^+-exchanged anthracene-loaded zeolite L suspended in a nonpolar organic solvent, which solubilizes anthracene.

There has been some confusion in the literature about different effects that have been reported to be supposedly observed on the same dye–zeolite materials. These differences are, according to our experience, often due to the fact that these systems were not the same, because they belong to one of the different categories explained above. The use of this terminology helps to more clearly specify the systems and, as a consequence, to better understand the experimental observations. We explain the different cases by discussing experimental results obtained for some cationic, neutral, and anionic dyes. Insertion of any dyes is carried out under conditions which characterize open systems. However, this also allows for a large variety of situations. We start by discussing some principles related to cationic dyes.

Cationic dyes: As the zeolite L framework is negatively charged and has charge-compensating cations within its structure, cationic chromophores can generally be inserted by ion exchange as follows: 1) Zeolite L is suspended in an appropriate solvent and 2) during stirring, the desired amount of dye dissolved in the same solvent is added. Depending on the dye, it might be necessary to heat the suspension, sometimes under reflux. The insertion time strongly depends on the properties of the dye, the size and shape of the crystals, and the desired final loading. We explain this for monovalent cationic dyes and monovalent charge-compensating cations. The principle remains the same if doubly charged cations are involved, but details may change considerably. The ion-exchange mechanism can be divided into two steps. First the monovalent cationic dye (D^+) dissolved

in water or another appropriate solvent (sol) is adsorbed to the external surface of the zeolite crystal (Z_S). If there are metal ions (M^+) available for exchange on the external surface of the zeolite, then ion exchange can take place as described in Equation (4).

$$n\mathrm{D}^+_{\mathrm{sol}} + (\mathrm{M}^+_{\mathrm{Z_s}})_{\mathrm{x}} \rightleftharpoons (\mathrm{M}^+_{\mathrm{Z_s}})_{\mathrm{x-n}}(\mathrm{D}^+_{\mathrm{Z_s}})_{\mathrm{n}} + n\mathrm{M}^+_{\mathrm{sol}} \quad (4)$$

It is also possible that the dye D^+ is adsorbed to the outer surface of the zeolite without ion exchange, which then gives rise to the alternative first step [Eq. (5)].

$$n\mathrm{D}^+_{\mathrm{sol}} + (\mathrm{D}^+_{\mathrm{Z_s}})_{\mathrm{y}} \rightleftharpoons (\mathrm{D}^+_{\mathrm{Z_s}})_{\mathrm{y+n}} \quad (5)$$

The dyes are inserted into the channels of zeolite L (Z_{ch}) in a second step. If ion exchange has taken place in the first step, Equation (4), no ion exchange occurs in the insertion equilibrium described by Equation (6). If no ion exchange has occurred in the first step [Eq. (5)], the second step is described by Equation (7). The overall ion exchange reaction is a mixture of both possibilities described above and can be expressed by Equation (8).

$$(\mathrm{D}^+_{\mathrm{Z_s}})_{\mathrm{n}} \rightleftharpoons (\mathrm{D}^+_{\mathrm{Z_s}})_{\mathrm{n-z}}(\mathrm{D}^+_{\mathrm{Z_{ch}}})_{\mathrm{z}} \quad (6)$$

$$(\mathrm{M}^+_{\mathrm{Z_{ch}}})_{\mathrm{x}}(\mathrm{D}^+_{\mathrm{Z_s}})_{\mathrm{y}} \rightleftharpoons (\mathrm{M}^+_{\mathrm{Z_{ch}}})_{\mathrm{x-n}}(\mathrm{D}^+_{\mathrm{Z_s}})_{\mathrm{y-n}}(\mathrm{D}^+_{\mathrm{Z_{ch}}})_{\mathrm{n}} + n\mathrm{M}^+_{\mathrm{sol}} \quad (7)$$

$$n\mathrm{D}^+_{\mathrm{sol}} + (\mathrm{M}^+_{\mathrm{Z_{ch}}})_{\mathrm{x}} \rightleftharpoons (\mathrm{M}^+_{\mathrm{Z_{ch}}})_{\mathrm{x-n}}(\mathrm{D}^+_{\mathrm{Z_{ch}}})_{\mathrm{n}} + n\mathrm{M}^+_{\mathrm{sol}} \quad (8)$$

To increase the dye concentration in the zeolite crystals, the equilibrium can be shifted towards the right side of Equation (8) by extracting M^+_{sol} from the reaction. This can be done by centrifuging the suspension and discarding the supernatant, which contains the cations, after partially loading the zeolites with dyes. The zeolites are then suspended in fresh dye solution to continue the loading. Another way to shift the equilibrium shown in Equation (8) to the right is by extracting the cations from the suspension by using a cryptand that selectively complexes those ions. This has been explained in references [12] and [29], in which we also described an interesting visual demonstration of the reactions given by Equations (5) and (6).

Thionine (ThH^+): An aqueous suspension of K^+-exchanged zeolite L crystals loaded with monoprotonated thionine corresponds to an open II system, because ThH^+, K^+, and H_2O can be freely exchanged. Conditions can be chosen such that the amount of dye at the outside (dissolved or adsorbed) is very low and negligible for the following discussion.[9] The absorption spectra of an aqueous solution of ThH^+ and of an aqueous dispersion of ThH^+-loaded zeolite L host–guest crystals are compared in Figure 3 (curves 1 and 3, respectively). We observe that the spectrum of the ThH^+-loaded zeolite L is slightly more structured and red-shifted by about 30 nm. Both changes are due to confinement effects.[9,30] There is not enough space for the formation of dimers inside the channels of zeolite L; however, the situation is different in the larger cavity of zeolite Y, in which formation of dimers has been observed.[31]

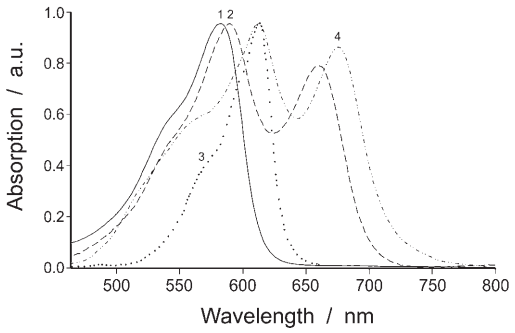

Figure 3. Absorption spectra of ThH^+ scaled to the same height at the maximum in: 1) Water; 2) 2.5 M HCl solution; 3) aqueous suspension of K^+-exchanged ThH^+-loaded zeolite L; and 4) aqueous suspension of H^+-exchanged ThH^+-loaded zeolite L. The concentration of ThH^+ was 10^{-5} M for the solutions. For the ThH^+–zeolite samples, the loading was 0.07 dye molecules per site.

Curve 4 of Figure 3 shows the spectrum of H^+-exchanged ThH^+-loaded zeolite L dispersed in water. We observe that encapsulation of ThH^+ in the acidic H-form of zeolite L generates a new band with a peak around 675 nm, which is due to the presence of the doubly protonated ThH_2^{2+}. The same band (blue-shifted) is exhibited by ThH^+ dissolved in 2.5 M HCl (curve 2). This shows that the acidity experienced by the ThH^+ in the channels of the H-form of zeolite L is equivalent to that of 2.5 M HCl. Because the extinction coefficients of ThH^+ at 590 nm and of ThH_2^{2+} at 660 nm are similar and the pK_{a2} of ThH^+ is -0.33, the similar intensities observed for those peaks (curves 2 and 4) indicates that the proton activity inside the H-form of zeolite L is approximately equivalent to a solution with pH -0.33.[9]

From the stoichiometry of a hydrated zeolite L, we see that the addition of one proton drastically increases the acidity inside the unit cell, because the H_3O^+/H_2O ratio becomes 1:21. This is close to the value of 0.047, calculated for a 2.5 M HCl solution. Because it is possible to exchange up to 3.6 cations per unit cell,[32] it is clear that the fully protonated H-form of zeolite L is a superacid. It is interesting that exchange of some K^+ ions by protons resulted in much faster insertion kinetics of ThH^+ from aqueous media, probably because ThH_2^{2+} is travelling faster than ThH^+.[9]

We emphasize that, for the systems under study, the terms acidity and proton strength should be preferentially used instead of pH, because of the very high ionic strength usually found inside the channels of zeolite L. It is nevertheless sometimes tempting to use the term pH. If, for example, curves 3 and 4 in Figure 3 are compared to curve 2, we can guess a pH of less than -0.3 inside the channels for the partially proton-exchanged zeolite, whereas we get pH >3 in the case of K^+-exchanged zeolite suspended in water. The situation is different when suspending the loaded zeolite L crystals in a buffer solution, because in this case the cations belonging to the buffer participate in the ion exchange equilibrium. It is also very different if the zeolite is dried in

vacuum and, for example, investigated under closed conditions, because protons are not solvated under these conditions.

A few dimers remaining at the outer surface of the zeolite do not affect the absorption spectra of the ThH^+-loaded zeolite L crystals suspended in water. When discussing fluorescence properties of dye–zeolite materials, however, each single dimer on a crystal can have an enormous effect and very efficiently quench the luminescence. The standard method to quantitatively eliminate such dimers from the outer surface is to wash the zeolite crystals, usually under semi-open III or semi-open IV conditions, with an appropriate solvent. This has been applied for preparing the OxH^+-loaded zeolite L samples, which we now discuss.

Oxonine (OxH^+): The two xanthene dyes OxH^+ and PyH^+ have been proven to be extremely useful for studying Förster energy transfer between randomly mixed donor–acceptor systems,[16b] for monitoring diffusion kinetics inside the channels of zeolite L by means of energy transfer,[33] and for developing fascinating antenna materials.[13,17] Both dyes are strongly luminescent in their monoprotonated form, OxH^+ and PyH^+, with quantum yields close to one, they are highly unstable in their deprotonated form, as expected for free amines, and both are nonfluorescent when doubly protonated. PyH^+ becomes colorless when doubly protonated, because the resonance is interrupted. Therefore, controlling the proton activity of this kind of system turns out to be very important.[34] We focus on OxH^+ rather than on PyH^+, because the protonation equilibrium of the former (see Figure 4, top) is fully reversible. We do not only have to consider protonation in the electronic ground state, but also in the first electronically excited singlet state, S_1. At pH 1, oxonine exists in the protonated form OxH^+, whereas in the S_1 state 60% of the molecules are doubly protonated. This means that excitation of OxH^+ at this pH gives rise to a fluorescence intensity which is approximately 60% less intense than that at pH 3, for example, at which more than 98% of the oxonine is monoprotonated in the S_1 state. This fluorescence quenching occurs because the protonation in the excited state is at least ten times faster than the fluorescence decay,[35,36] which has a fluorescence rate constant of $3\times10^8\ s^{-1}$ for OxH^+.[37] This is confirmed by a comparison between the fluorescence spectra of aqueous solutions of OxH^+ at pH 3 and 1 (Figure 4, bottom), the latter showing about 60% less intensity.

In loaded zeolite samples, the quenching through energy transfer is much stronger because the distance between the molecules in these materials is small. Besides, the absorption spectrum of OxH_2^{2+} is similar to that of OxH^+, which allows an efficient energy transfer from $(OxH^+)^*$ to the nonfluorescent OxH_2^{2+}. Therefore, the quenching caused by OxH_2^{2+} can be very severe.

Methods for preparing standing zeolite L crystals on a substrate have been recently developed.[17,20] A convenient method for this is to first modify a glass or quartz substrate with triethoxysilane derivatives and then to attach the zeolite. HCl is produced upon the reaction of the zeolite with the modified surface; for details see reference [17]. This can be seen when loading the zeolite monolayer prepared in this way with OxH^+, immersing the sample in toluene, and measuring the absorption spectrum.[13] A new absorption band at 640 nm is observed, as shown by the arrow in Figure 5 (top). The same band appears when dissolving OxH^+ in a 2.5 M HCl solution; however, it is much weaker (Figure 5, bottom, solid line). This means that the acidity inside the channels of the zeolite L monolayer is higher than that of 2.5 M hydrochloric acid. The acidity of the system is conserved because the toluene is unable to accept the protons from the zeolite. The system "OxH^+-loaded zeolite L monolayer", when immersed in toluene, can be regarded as a semi-open II system. Controlled adjustment of the pH is, however, possible by a short immersion of the sample in an alkaline ethanol solution (semi-open IV system). Referring back to toluene and again measuring the absorption spectrum shows that the peak at 640 nm has disappeared as a result of the neutralization reaction (Figure 5, top, dotted line).

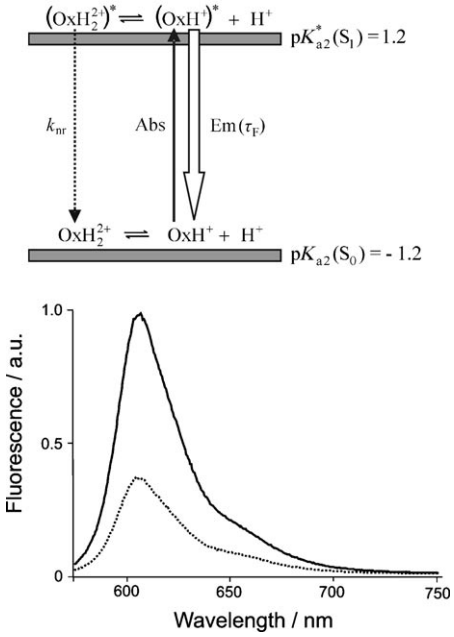

Figure 4. Top: Energy diagram showing the second protonation of oxonine in the ground state S_0 and in the excited singlet state S_1. At pH 1 mostly OxH^+ is present in the S_0 state (>99%), but after absorption the population of the diprotonated form is about 60%, leading to the loss in the fluorescence intensity through the nonradiative decay k_{nr} of OxH_2^{2+}. Bottom: Comparison between the fluorescence spectra of aqueous solutions of oxonine at pH 3 (——) and pH 1 (•••••). $c=2\times10^{-6}$ M, $\lambda_{exc}=550$ nm, $T=298$ K.

Dsm^+: This dye works nicely as a Brønsted acidity probe for the interior of zeolite L, because the ratio between the absorbances of Dsm^+ ($\lambda_{max}=450$ nm) and its protonated form, $DsmH^{2+}$ ($\lambda_{max}=330$ nm), allows the accurate determination of the proton activity (Figure 6) and its pK_{a1} is appropriate for a frequently used acidity range. Better under-

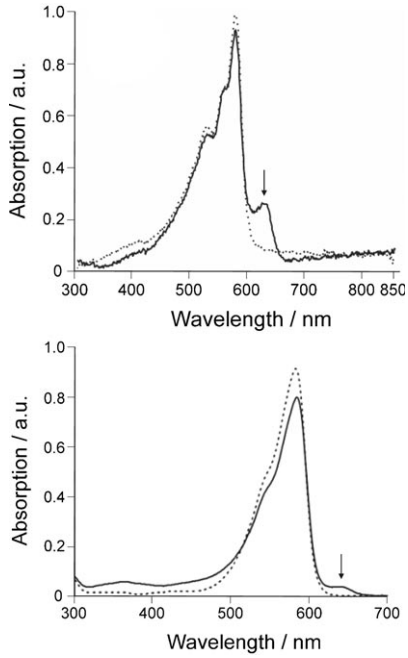

Figure 5. Top: Absorption spectra of partially H^+-exchanged OxH^+-loaded zeolite L monolayer in toluene, before (——) and after (•••••) short immersion in an alkaline ethanol solution. The loading of OxH^+ is 0.012 dye molecules per site. The arrows indicate the position where OxH_2^{2+} absorbs (640 nm). Bottom: Absorption spectra of 3×10^{-6} M solutions of OxH^+ in water (•••••) and in 2.5 M HCl solution (——). $T=$ 298 K.[13]

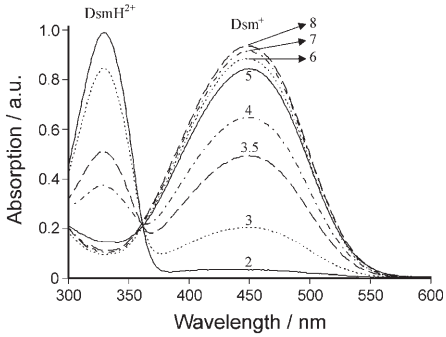

Figure 6. Absorption spectra of aqueous solutions of Dsm^+ at different pH values ranging from 2 to 8. The bands around 330 and 450 nm correspond to $DsmH^{2+}$ and Dsm^+, respectively. $c=10^{-5}$ M and $T=298$ K. The extinction coefficients are 34600 and 43660 $M^{-1}cm^{-1}$ for Dsm^+ (450 nm) and $DsmH^{2+}$ (330 nm), respectively.

standing of the behavior of this dye in the cavities of zeolites is also of interest in connection with recent research on second-order harmonic generation zeolite films.[38]

Diffuse transmission spectra of M-exchanged Dsm^+-loaded zeolite L crystals (M: K^+, Li^+, Cs^+, Mg^{2+}, Ca^{2+}) dispersed in water have been recorded and the ratio between the bands of $DsmH^{2+}$ and Dsm^+ were used to estimate the proton activity inside a fully hydrated zeolite L. This allowed the investigation of the influence of the zeolite counterion on the proton activity of the Brønsted sites. The results are shown in Table 2, together with the pK_a values of aqueous solutions of the corresponding metal ions.

Table 2. The pK_a values of aqueous solutions of metal ions (M) compared to the pH values estimated inside Dsm^+-loaded M-exchanged zeolite L crystals dispersed in water at 298 K.[12a]

Exchanged cation (M)	pK_a	pH inside the zeolite
Li^+	13.6	3.45
K^+	14.0	3.38
Cs^+	–	3.68
Mg^{2+}	11.2	2.82
Ca^{2+}	12.7	3.10

The differences observed among the counterions can be interpreted through acid–base reactions with water. It is well known that metal cations give acidic solutions when dissolved in water, according to Equation (9):[39]

$$[M(H_2O)_n]^{m+} + H_2O \rightleftharpoons [M(H_2O)_{n-1}(OH)]^{(m-1)+} + H_3O^+ \quad (9)$$

These pH changes, which depend on the nature of the cation (see pK_a values in Table 2), explain the difference in acidity inside the Dsm^+-loaded zeolite L crystals. Zeolites exchanged with Mg^{2+} showed the strongest proton activity, in agreement with its small pK_a value.

In another experiment, K^+-exchanged Dsm^+-loaded zeolite L crystals were suspended in different buffers and their diffuse transmission spectra were recorded, allowing the estimation of the proton activity (Figure 7). The estimated pH values inside the zeolite L were 3.29, 3.34, 3.56, and 3.63, corresponding to the buffers with pH 5, 6, 7, and 9, respectively. It is interesting to note that, although the pH of the buffers varied by four pH units, the pH estimated inside the zeolite remained nearly constant. This is because the cations belonging to the buffers participate in the ion-exchange equilibrium of this semi-open IV system.

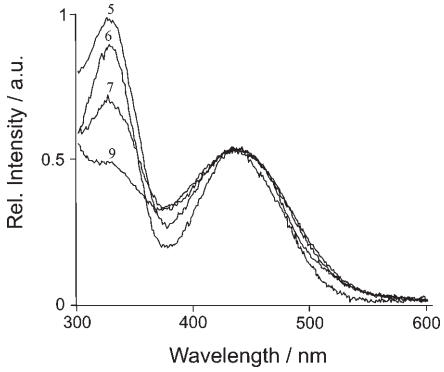

Figure 7. Diffuse transmission spectra of K^+-exchanged Dsm^+-loaded zeolite L crystals suspended in aqueous buffer solutions, the pH values of which are indicated for each case. The Dsm^+ loading is 0.05 dye molecules per site. For comparison purposes the intensity of the band at 450 nm was kept constant. $T=298$ K.

Neutral dyes: Having discussed host–guest materials based on cationic guest molecules, in which we have to deal with semi-open III and semi-open IV systems, we now turn to materials based on neutral guests, in which semi-open I and semi-open II situations are often found.

Hostasol Red (HR): Protonation of HR can only occur in a very acidic medium. This compound shows strong fluorescence in a 1:3 acetone/water mixture at neutral pH or under slightly acidic conditions with a maximum at 615 nm, whereas a much weaker emission around 650 nm is observed at a pH of zero. The molecule can be easily inserted into vacuum-dried zeolite L from the gas phase by means of sublimation. Samples prepared with different zeolite L crystals containing K^+, Cs^+, and Mg^{2+} as charge-compensating cations (M) show different luminescence intensities, depending on M, which strongly influences their color. We show in Figure 8 three samples inside sealed evacuated glass ampoules at about 10^{-2} mbar at room temperature. The most intense luminescence by far of HR-loaded zeolite L is observed in the Cs^+-exchanged zeolite, it is medium for K^+-, and weakest for the Mg^{2+}-exchanged sample.

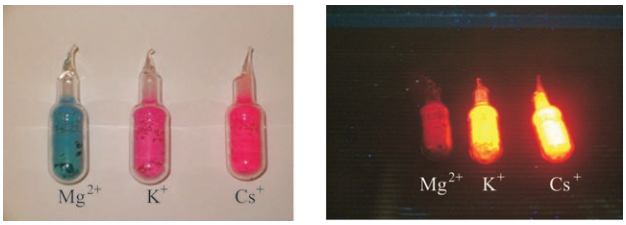

Figure 8. Color of M-exchanged HR-loaded zeolite L samples (left), and the same samples under excitation at 366 nm (right) observed at RT. M: Mg^{2+}, K^+, and Cs^+; the HR loading is 0.05 dye molecules per site.

These samples can be classified as closed systems, because they are inside the ampoules. The nature of the counterion evidently plays an important role. It would be tempting to attribute the differences shown in Figure 8 to specific HR–cation interactions, by forgetting the protons remaining inside the channels, which may also influence the behavior of those systems. The strong luminescence exhibited by the samples with Cs^+ as counterion is blue-shifted with respect to the other samples, and the same strong emission is observed in a 1:3 acetone/water mixture solution of HR at pH 5, in which no Cs^+ ions are present. Therefore, the strong luminescence observed for Cs^+-exchanged HR-loaded zeolite L cannot be attributed to the heavy-atom effect. It seems, however, that the different behavior of the three samples correlates with the different acidity inside the zeolite L channels, which, according to Table 2, increases in the order $Cs^+ < K^+ \ll Mg^{2+}$. We should be aware that these changes are larger under closed conditions than under, for example, semi-open III conditions, under which ion exchange can take place. Measuring proton strength and proton mobility in such samples is not easy, but one has nevertheless some understanding in this matter.[40] The pK^*_{a1} of HR is in the order of 1.5. This means that in the excited state HR can be partially protonated at pH 2. Therefore, it makes sense to assume that the acidity in the Mg^{2+}-exchanged zeolite L is such that efficient protonation in the excited state takes place, causing efficient luminescence quenching. The acidity of K^+-exchanged zeolite L is closer to that of Cs^+-exchanged samples, so that much less quenching takes place.

We did the following experiments to further test the validity of this interpretation. Proton hopping is relatively slow in dry zeolite L. However, excited-state protonation is expected to be more efficient if the protons have a high mobility, because it must take place within the lifetime of the excited state. Proton mobility is greatly increased in the presence of some water molecules.[4] The number of water molecules inside the zeolite can be reduced by evacuating the system under semi-open II conditions. This can be used to investigate their influence on the luminescence quenching of the encapsulated HR. Experiments were carried out at room temperature for K^+-exchanged samples in an apparatus described[41] which allows us to monitor the pressure and hence the vapor pressure of water. The effect is that the luminescence of the sample is strongly increased and blue-shifted upon evacuation, as seen in Figure 9 (top).

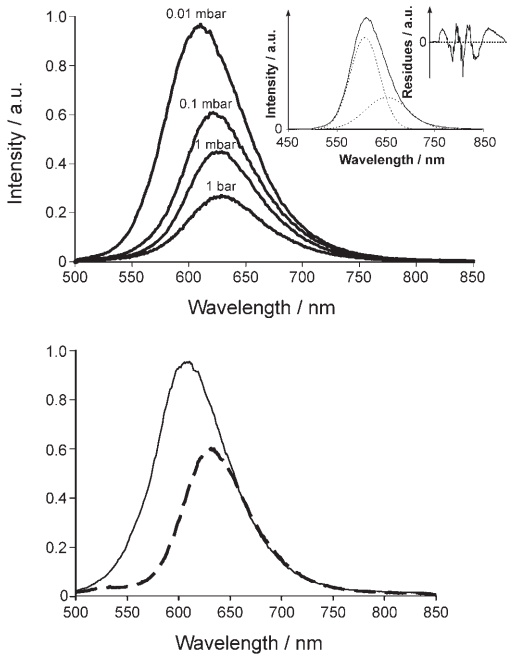

Figure 9. Top: Fluorescence spectra of K^+-exchanged HR-loaded zeolite L crystals obtained by gradually evacuating the air-equilibrated sample, which was in the powder form. The inset shows the deconvolution of the emission spectrum at 0.01 mbar (——) into 2 Gaussians (– – –) and the random distribution of the residues; Bottom: Emission spectra of the same HR-loaded zeolite L samples at 7×10^{-4} mbar (——) and after increasing the pressure to 1 mbar upon exposure to water vapor (– – –). The HR loading = 0.015 dye molecules per site, $\lambda_{exc} = 473$ nm, $T = 298$ K. The water was previously degassed by the pump-freeze-thaw technique.

Deconvolution of the emission spectrum (Figure 9, inset) shows two bands which may be attributed to the emission of the HR ($\lambda_{max} \approx 600$ nm) and emission of perturbed HR, perhaps HR protonated in the excited state ($\lambda_{max} \approx 650$ nm). The small contribution of the band at 650 nm obtained from the deconvolution is indicative of a low water content at 0.01 mbar, which causes a considerable decrease in the proton mobility. We observed that dipping the HR-loaded zeolite L crystals in a 0.1 M NaOH aqueous solution for a few seconds, similarly to the procedure carried out for OxH^+, causes a blue shift in the emission and an increase of the intensity by about a factor of two in all cases. This supports the interpretation that the main factors influencing the fluorescence behavior of HR inside the zeolite L are the concentration and mobility of the protons.

Figure 9 (bottom) shows the emission spectra of K^+-exchanged HR-loaded zeolite L initially evacuated at 7×10^{-4} mbar (solid line) and after adding degassed water vapor to reach 1 mbar (dashed line). These wet and dry situations correlate well with the two Gaussians obtained by deconvolution of the emission spectrum of the same system at 0.01 mbar (Figure 9, inset).

Reversible color changes have been observed upon varying the water content of *p*-nitroaniline-loaded zeolite Y and mordenite, depending on the kind of charge-compensating cations M equal to Li^+, Na^+, K^+, Rb^+, and Cs^+.[42] The changes of the absorption spectra were attributed to the different interactions of the dyes with the metal cations, which were shown to depend on the water content. Full hydration of the cations diminishes direct interaction with the encapsulated dyes.

The influence of proton transfer in the excited state has also been studied for 3-hydroxyflavone (3-OHF) synthesized by means of a ship-in-a-bottle procedure in zeolite β. 3-OHF shows two emission bands in ethanol, corresponding to the two excited-state isomers N* and T*, whereas only the emission band of N* 3-OHF is observed inside the zeolite β, providing evidence for the protic/polar environment of the zeolite β cavity.[43]

JCG65: This dye can assume the *cis* and *trans* forms (relative to the double bond of the aliphatic nitrogen, see Scheme 2), but only the latter is able to enter into the zeolite L channels because of spatial restrictions. In solution, the absorption spectrum of JCG65 exhibits an intense and broad band at 425 nm, which corresponds to the neutral form, and at pH > 9 a new absorption band of the deprotonated dye appears at 575 nm (see Figure 10).

The small shoulder at around 507 nm disappears at pH < 3.4, and also in the spectrum of the encapsulated form, indicating that this band may be due to the *cis* form, which cannot be encapsulated. The lack of an isosbestic point around 500 nm in Figure 10 is due to the absence of a 1:1 stoichiometry between protonated and deprotonated JCG65, because more than one isomer is involved in the acid–base equilibrium. On the other hand, a clear isosbestic point is seen at $\lambda = 344$ nm (Figure 10, arrow), which is removed upon addition of HCl. The assignment of the absorption bands shown in Figure 10 is discussed in more detail in the section on molecular orbital calculations.

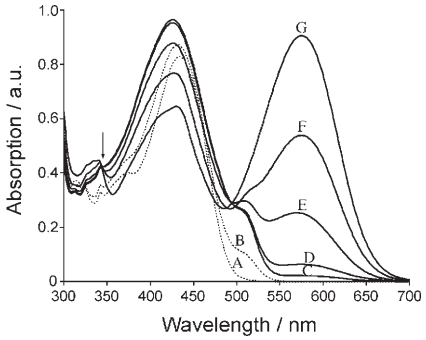

Figure 10. Absorption spectra of JCG65 in DMSO at different pH values, $c = 1.4 \times 10^{-4}$ M and $T = 298$ K. Curve C represents the initial JCG65 solution, the other curves being produced by addition of HCl (curves A and B) or NaOH (curves D, E, F, and G). The measured pH values of the solutions were: A) 2.3, B) 3.4, C) 9.1, D) 9.8, E) 11.2, F) 12.0, and G) 13.0. The arrow indicates an isosbestic point ($\lambda = 344$ nm), which involves only the alkaline solutions.

Encapsulation of JCG65 inside the zeolite L gives rise to a single absorption band peaked around 425 nm (Figure 11, solid line). The same band is observed for the NG43 dye, the structure of which is similar to that of JCG65, the only difference being the naphthalene moiety, which is present in JCG65, but absent in NG43. By comparing the structures and absorption spectra of both dyes, it turns out that the absorption band at 425 nm observed for JCG65 is localized in the naphthalimide moiety.

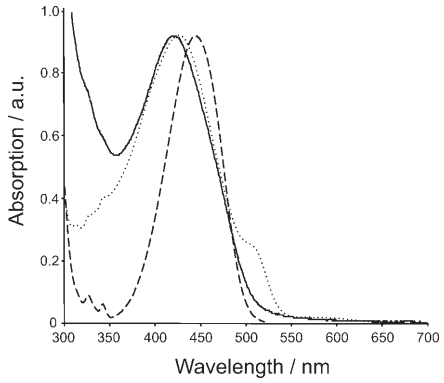

Figure 11. Absorption spectra of JCG65 in DMSO (•••••), JCG65 inside K^+-exchanged zeolite L crystals suspended in ethyl benzoate (——) and NG43 in DMSO (– – –). The loading of JCG65 inside the zeolite L is 0.5 dye molecules per site. $c = 4.7 \times 10^{-5}$ M and 1.4×10^{-4} M for the NG43 and JCG65 solutions, respectively. $T = 298$ K.

The K^+-exchanged JCG65-loaded zeolite L crystals suspended in ethyl benzoate (Figure 11) correspond to the semi-open I system, because the cations cannot be accepted by the nonpolar ethyl benzoate, and JCG65 does not leave free space for the diffusion of the bulky ethyl benzoate. If one added to this suspension a crown ether specific for K^+

ions, the system would be characterized as semi-open III, because the counterion could now be exchanged.

The absorption spectrum of JCG65 inside the zeolite L is very similar to curve A of Figure 10, which then indicates that the proton activity experienced by JCG65 inside the zeolite corresponds to a pH value smaller than 3.4 (curve B) and higher than 2.3 (curve A).

Solvent Green 5 (SG5): It has been observed that the absorption spectra of SG5 exhibit a strong change when the SG5 is encapsulated inside the K^+-exchanged zeolite L. In contrast to the previous cases discussed, the spectral change is caused by an acid hydrolysis occurring inside the zeolite, during which isobutanol is produced (see Scheme 2). Addition of SG5 to HCl or NaOH aqueous solutions leads to the hydrolysis of the dye, resulting in the disappearance of the absorption band around 480 nm and appearance of a weak absorption band around 400 nm. The absorption spectra of both acidic and basic hydrolyzed species exhibit the same shape, as expected.

Figure 12 shows a comparison between excitation and emission spectra of a solution of SG5 in ethanol and K^+-exchanged SG5-loaded zeolite L crystals dispersed in ethanol. The dispersion in ethanol is characterized as an open II system.

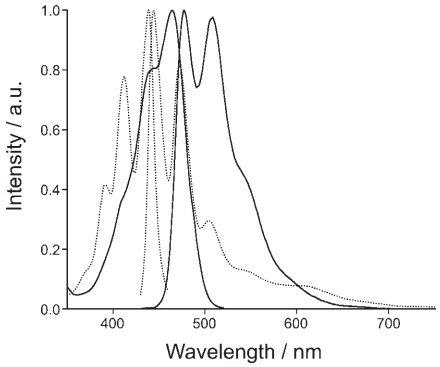

Figure 12. Excitation and emission spectra of K^+-exchanged SG5-loaded zeolite L crystals suspended in ethanol (•••••) and of a 1.7×10^{-5} M SG5 ethanolic solution (——). For the emission spectra $\lambda_{exc}=410$ nm and for the excitation spectra $\lambda_{em}=510$ nm. The loading of SG5 inside the zeolite crystals was 0.8 dye molecules per site. $T=298$ K.

The results show that, once inside the zeolite L, the SG5 dye is irreversibly hydrolyzed, the excitation and emission spectra being always the same. The reaction back to the initial ester form of SG5 is hampered, because the aromatic part of the species formed has a much stronger interaction with the zeolite L, whereas the small isobutanol molecules formed can diffuse much more easily through the channels and escape. The same does not occur in solution, in which the initial absorption spectrum of SG5 can be restored by adding H_2SO_4 to a solution of SG5 in ethanol previously hydrolyzed by addition of KOH.

The excitation spectrum of the encapsulated SG5 (Figure 12, dotted line) also remains the same after dipping the SG5-loaded zeolite L crystals in HF, under which conditions the zeolite framework is dissolved.

Other chemical reactions inside zeolites have been detected through the change in the absorption or emission spectra of the loaded crystals. Spectral changes observed in ZSM-5 single crystals loaded with furfuryl alcohol molecules, for example, have been attributed to a polymerization reaction involving those molecules.[44] Also, luminescence quenching through electron transfer of $[Ru(bpy)_3]^{2+}$ by methyl viologen, both encapsulated inside the zeolite X or Y, has been monitored by means of confocal microscopy of a single crystal.[45] A variety of interesting photochemical reactions inside zeolites has been recently reviewed.[46]

Anionic dyes: Little is known about anionic dyes inside zeolite L and other zeolites, because the anionic framework does not easily accept anions. Special procedures are needed for preparing and stabilizing such systems. The best studied example is Resorufin-loaded zeolite L.[45,47]

Resorufin (ResH): This dye presents absorption maxima at 480 nm in the protonated form, ResH. The deprotonation of Resorufin to form the Res^- species gives rise to a new absorption band with fine structure peaked around 578 nm.[47] The absorption spectra of both forms in ethanol and of K^+-exchanged ResH-loaded zeolite L crystals are shown in Figure 13. The absorption spectrum of the encapsulated

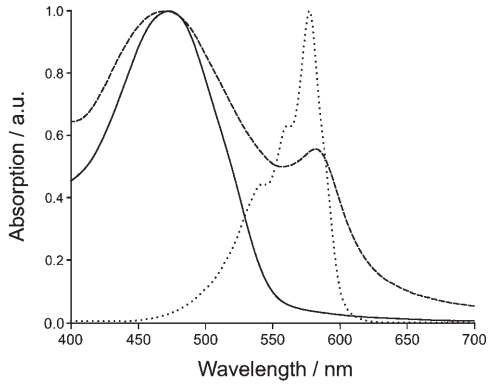

Figure 13. Normalized absorption spectra of ResH (——) and Res^- (•••••) in ethanol at the concentration of about 10^{-5} M and of K^+-exchanged ResH-loaded zeolite L crystals suspended in CH_2BrCl (dashed line) after washing the crystals with ethanol. Loading = 0.07 dye molecules per site, $T=298$ K.

ResH (Figure 13, dashed line) clearly shows that washing the K^+-exchanged ResH-loaded zeolite L crystals with ethanol leads to deprotonation of Resorufin, because the band characteristic of Res^- is also present around 580 nm. A much more efficient deprotonation of the encapsulated ResH is usually made by dipping the loaded zeolite L crystals in a 0.2 M KOH solution, after which the band at 480 nm completely disappears. This procedure can be performed for

open systems, although it is more efficient for the semi-open IV ones, in which proton exchange occurs, as the dye remains inside the zeolite. Because the pK_a of Resorufin is 5.5, and the ratio between the bands at 480 nm (ResH) and 580 nm (Res^-) is around two (Figure 13, dashed line), one can estimate the pH inside the K^+-exchanged zeolite L after washing with ethanol to be approximately 5.2. This value larger than those estimated with Dsm^+ (see Table 2). This may be attributed to the washing with ethanol, which perhaps decreases the proton activity inside the zeolite. The oscillator strengths of Res^- and ResH are very similar.[47]

Although both ResH and Res^- forms are luminescent, Res^- is completely quenched when encapsulated into K^+-exchanged zeolite L crystals. Interestingly, encapsulation of Res^- into Li^+-exchanged zeolite L crystals reestablishes its luminescence. This may be attributed in part to the heavy-atom effect, which is known to decrease or even extinguish the fluorescence of dye-loaded zeolites upon increasing the atomic number of the counterion.[14] For example, the intensity ratio $I_{Phosphorescence}/I_{Fluorescence}$ in dry naphthalene-loaded zeolite X increases 1600 times upon changing the Li^+ counterion by K^+.[48]

Molecular orbital calculations

Hostasol Red (HR): Extended Hückel molecular orbital calculations were found to be appropriate for discussing the frontier orbitals of HR as configuration interaction plays a minor role in this case. The so-obtained molecular orbital diagram of HR is shown in Figure 14.

The HOMO→LUMO excitation has π*←π character. The frontier orbitals illustrated in Figure 14 and the charge distribution in Scheme 3 show that electron density is shifted from the sulfur to the carbonyl group upon this electronic excitation. This supports the interpretation that protonation of the excited singlet state of the Hostasol is expected to occur in the oxygen of the carbonyl group, as shown in Scheme 2, and explains why protonation of HR in the S_1 state is possible at moderate pH.

JCG65: The structures of the *cis* and *trans* isomers of JCG65 have been optimized with the semiempirical AM1 method[49] and exhibit very similar energies. The excited singlet states have been calculated with the ZINDO/S method[50] by using configuration interaction with single excitations within an active window of 40 occupied versus 40

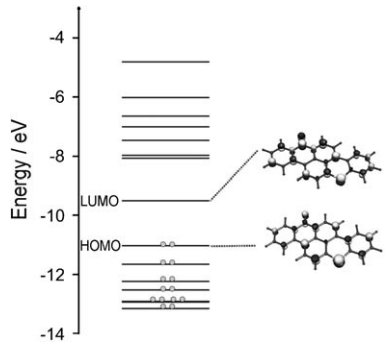

Figure 14. Molecular orbital diagram of HR and molecular orbitals of the HOMO and the LUMO.

unoccupied molecular orbitals. The oscillator strengths and energies of the transitions to the first excited singlet (S_1←S_0) of JCG65 are shown in Table 3, in which the labels *trans*$^-$ and *cis*$^-$ represent the deprotonated species.

The theoretical results shown in Table 3 have been used to assign the bands in the absorption spectra of JCG65. Comparison between the experimental absorption spectra of

Table 3. Calculated oscillator strengths and wavelengths of the electronic transitions to the lowest excited singlet of JCG65 in the different isomer and protonated/deprotonated forms.

Isomer	$\lambda_{S1←S0}$ [nm]	Oscillator strength	Transition type[a]
trans	372	1.03	π*←π
trans$^-$	525	1.06	π*←π
cis	348	0.56	π*←π
cis$^-$	507	0.53	π*←π

[a] These transitions are mainly HOMO→LUMO in character.

JCG65 in DMSO at different pH values and the calculated transition energies and oscillator strengths is shown in Figure 15, in which the vertical bars represent the electronic transitions given in Table 3 and their heights have been scaled with the respective oscillator strengths. The intense absorption bands centered around 425 and 575 nm (Figure 15, solid line) stem from the *trans* and *trans*$^-$ isomers, respectively. The shift observed between the experimental and calculated values are assumed to arise from the solvent effect, which was not taken into account in the calculations. The shoulders on the left side of both bands may be due to the *cis* and *cis*$^-$ species. The attribution of these

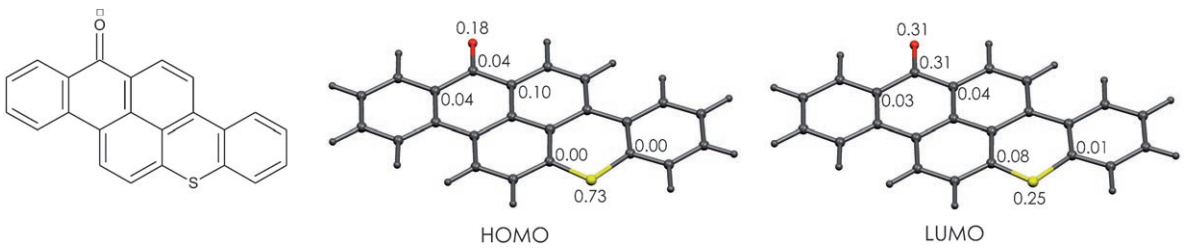

Scheme 3. Atomic partial charges of the HOMO and LUMO orbitals of HR.

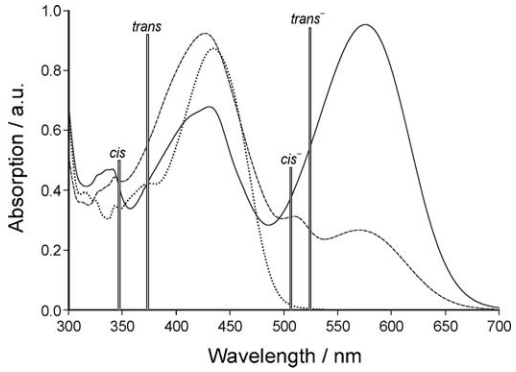

Figure 15. Comparison between the absorption spectrum of JCG65 in DMSO at pH 13.0 (——), 11.2 (– – –), and 2.3 (•••••), and the calculated oscillator strengths and transition energies of this dye (vertical bars). The height of the bars is given by their respective oscillator strengths.

shoulders is, however, not trivial, because keto–enol tautomerism may also play a role in this case.

The decrease of the pH of the JCG65 solution (Figure 15, dashed line) causes partial protonation of the *trans*$^-$ and *cis*$^-$ species, decreasing the intensity of their respective absorption bands, as well as of the shoulder observed around 400 nm. Further decrease of the pH to a value of 2.3 (Figure 15, dotted line) causes the absorption bands of the *trans*$^-$ and *cis*$^-$ and of the shoulder at 400 nm to completely disappear. The remaining band centered at 425 nm is also observed upon encapsulation of JCG65 into the zeolite L (see Figure 11, solid line), indicating that only the *trans* isomer can be encapsulated.

The absorption band assigned to the *trans* form ($\lambda \approx 425$ nm) is also observed in solutions of the NG43 dye, the chromophore of which is similar to that of JCG65 (see Scheme 2), in DMSO. This indicates that the absorption band of JCG65 is localized in the moiety containing the imide group. In fact, a linear combination between the HOMO and HOMO−1 molecular orbitals of JCG65 can be used to show that its $S_1 \leftarrow S_0$ transition is indeed localized in that part of the molecule, as shown in Figure 16.

Conclusions

Zeolite L crystal samples partially exchanged with protons exhibit proton activity higher than that of 2.5 M HCl solutions and can even be regarded as being superacids. The pH inside the fully hydrated, M-exchanged, Dsm$^+$-loaded zeolite L crystals (M: K^+, Li^+, Cs^+, Mg^{2+}, Ca^{2+}) ranges from about 2.5 to 3.5, whereas it is less than −0.33 for partially proton-exchanged, OxH$^+$-loaded zeolite L. In particular, the differences observed in the estimated pH inside the Dsm$^+$-loaded zeolite L samples are attributed to an acid–base reaction of the metal cations with water, which is known to increase the acidity of aqueous media.

Evacuation of dye-loaded zeolite L crystals, which changes the water content and therefore the proton mobility inside the channels, directly changes the proton activity, as has been shown by an efficient excited-state protonation observed for HR-loaded zeolite L samples. This interpretation is reinforced by measurements carried out for Hostasol Yellow (HY, see Scheme 2), which has a similar structure to that of HR, the only difference being that the carbonyl group of the imide group present in HY does not influence the aromatic conjugation as does the carbonyl group in HR. As a result, excited-state protonation is not observed in HY solutions.

The proton activity of both H$^+$-exchanged and M$^+$-exchanged dye-loaded zeolite L crystals can be tuned by immersion in an alkaline solution, as has been illustrated for different dyes. Although this has been done for open systems, fine tuning of the proton activity may be achieved by using semi-open III or IV systems, in which cation diffusion may be slower depending on the stopcock used. This treatment allows fine tuning and hence control of the spectroscopic properties of encapsulated dyes.

In summary, we have studied the proton activity inside the channels of zeolite L by investigating the influence on the spectroscopic properties of encapsulated dyes under different conditions, such as the water content inside the zeolite, nature of the counterion, and nature of the solvent of the dispersion. The systems investigated have been divided into closed, semi-open, and open types, which express their

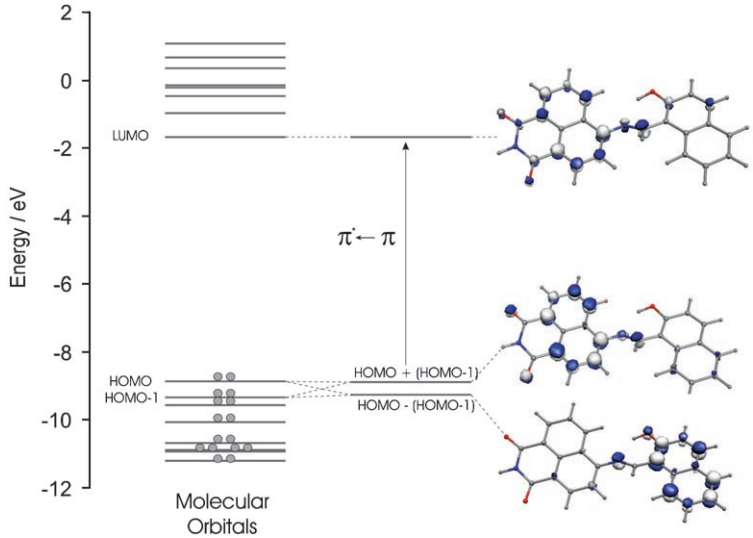

Figure 16. Molecular orbital diagram of the *trans* isomer of the JCG65 dye calculated by using the AM1 method. The two lower molecular orbitals shown on the right side are linear combinations of the HOMO and HOMO−1 orbitals.

ability to exchange matter with the chemical environment outside the zeolite. This ordering has been found to be very useful to improve our understanding of dye–zeolite host–guest materials and hence to better control their properties.

Experimental Section

Materials: Zeolite L was synthesized according to the procedure described.[51] The dyes JCG65, HR, and SG5 were provided by Clariant GmbH. Resorufin was synthesized according to the description of Eichler.[52] Pyronine was synthesized following the description of Müller.[53] Oxonine was synthesized according to reference [54]. Dsm^+ was purchased from the company Micro Probes. Thionine was obtained by converting its hydrochloride form, purchased from Merck, to the free base, according to the procedure described in reference [9]. The solvents used were toluene (Fluka, puriss), DMSO (Merck, Uvasol), ethanol (Merck, Uvasol), CH_2BrCl (Fluka, purum), and ethyl benzoate (Fluka, purum). The following buffer solutions were used: pH 1 (0.13 M HCl, 0.05 M KCl), pH 2 (0.03 M citric acid, 0.0082 M HCl, 0.061 M NaCl), pH 3 (0.04 M citric acid, 0.21 M NaOH, 0.06 M NaCl), pH 5 (0.096 M citric acid, 0.2 M NaOH), pH 6 (0.06 M citric acid, 0.16 M NaOH), pH 7 (0.029 M NaOH, 0.05 M KH_2PO_4).

Oriented zeolite L monolayer: Zeolite L crystals were covalently bound to a glass substrate functionalized with (3-chloropropyl)trimethoxysilane, as described in reference [17].

Dye-loaded zeolite L: The cationic dyes (oxonine, pyronine, thionine, and Dsm^+) were inserted through ion exchange with the counterions of K^+-exchanged zeolite L crystals in aqueous solution. The neutral dyes (Hostasol Red, JCG65, and Solvent Green 5) were inserted in the gas phase. Resorufin was inserted in the gas phase and then the loaded zeolite L crystals were dipped in a KOH solution to generate the deprotonated form.[47] The procedures of gas-phase and ion-exchange insertion are described in reference [12]. The samples shown in Figure 8 were prepared by first drying 80 mg of the sample under vacuum for 2 h at 150 °C, sealing the ampoules, and loading for 48 h, at 250 °C.

Spectroscopic measurements: The absorption spectra were recorded by using a Perkin–Elmer Lambda 900 UV/Vis spectrometer. Excitation and emission spectra were recorded by using a Perkin–Elmer LS 50B luminescence spectrometer.

Low-pressure measurements: The emission was measured at low pressure by using a high-vacuum chamber described in reference [41] by using an Alcatel turbomolecular vacuum pump, model Drytel 1025. The acquisition of the spectra was carried out on a system consisting of a Nd:YAG pulsed laser (Quantel Brilliant) and an OPO (Opotek MagicPrism Vibrant Vis), which was pumped by the third harmonic. The pulse length was 5 ns.

Molecular orbital calculations: The Extended Hückel molecular orbital calculations were carried out by means of the ICON-EDiT program,[55] whereas all the other quantum chemical calculations were carried out by using the Hyperchem 7.51 program.[56]

Acknowledgements

We would like to acknowledge Dr. Stefan Huber for providing the experimental data reported in Figures 4 and 5, Le-Quyenh Dieu for her contributions regarding JCG65, André Mätzener, Christian Eyholzer, and Simon Fahrni for contributing to the data reported in Figures 8, 9, and 12, respectively. We would like to thank René Bühler for his contributions to several experiments, mainly to the data reported in Figures 10 and 11. The financial support by the Swiss Federal Office of Energy (project 101783) and by the Schweizerische Nationalfonds zur Förderung der wissenschaftliche Forschung SNSF (project number 200020-105140) is gratefully acknowledged. We also thank Clariant GmbH for providing some of the dyes used in this work.

[1] W. E. Farneth, R. J. Gorte, *Chem. Rev.* **1995**, *95*, 615–635.
[2] R. M. Barrer, *Zeolites and Clay Minerals as Sorbents and Molecular Sieves*, Academic Press, London, **1978**.
[3] "Intrazeolite Chemistry": G. W. Skeels, W. H. Flank, *ACS Symp. Ser.* **1983**, *218*, 369–382.
[4] J. A. Ryder, A. K. Chakraborty, A. T. Bell, *J. Phys. Chem. B* **2000**, *104*, 6998–7011.
[5] D. T. Chen, S. B. Sharma, I. Filimonov, J. A. Dumesic, *Catal. Lett.* **1992**, *12*, 201–212.
[6] a) M. Hunger, D. Freude, D. Fenzke, H. Pfeifer, *Chem. Phys. Lett.* **1992**, *191*, 391–395; b) P. Batamack, C. Doremieux-Morin, J. Fraissard, *J. Chim. Phys.* **1992**, *89*, 423–433.
[7] H. G. Karge, V. Dondur, J. Weitkamp, *J. Phys. Chem.* **1991**, *95*, 283–288.
[8] A. Zecchina, G. Spoto, S. Bordiga, *Phys. Chem. Chem. Phys.* **2005**, *7*, 1627–1642.
[9] G. Calzaferri, N. Gfeller, *J. Phys. Chem.* **1992**, *96*, 3428–3435.
[10] a) S. Corrent, P. Hahn, G. Pohlers, T. J. Connolly, J. C. Scaiano, V. Fornés, H. García, *J. Phys. Chem. B* **1998**, *102*, 5852–5858; b) S. Y. Choi, Y. S. Park, S. B. Hong, K. B. Yoon, *J. Am. Chem. Soc.* **1996**, *118*, 9377–9386.
[11] U. Eichler, M. Brändle, J. Sauer, *J. Phys. Chem. B* **1997**, *101*, 10035–10050.
[12] a) G. Calzaferri, S. Huber, H. Maas, C. Minkowski, *Angew. Chem.* **2003**, *115*, 3860–3888; *Angew. Chem. Int. Ed.* **2003**, *42*, 3732–3758; b) M. Pauchard, A. Devaux, G. Calzaferri, *Chem. Eur. J.* **2000**, *6*, 3456–3470; c) A. Devaux, C. Minkowski, G. Calzaferri, *Chem. Eur. J.* **2004**, *10*, 2391–2408.
[13] a) G. Calzaferri, S. Huber, A. Devaux, A. Zabala Ruiz, H. Li, O. Bossart, L.-Q. Dieu, *Proc. SPIE—Int. Soc. Opt. Eng.* **2006**, *6192*, 619216; b) S. Huber, A. Zabala Ruiz, H. Li, G. Patrinoiu, C. Botta, G. Calzaferri, *Inorg. Chim. Acta* **2007**, *360*, 869–875.
[14] V. Ramamurthy in *Photochemistry in Organized and Constrained Media*, (Ed.: V. Ramamurthy), VCH, New York, **1991**, pp. 429–493.
[15] a) Ch. Baerlocher, W. M. Meier, D. H. Olson, *Atlas of Zeolite Framework Types*, 5th ed., Elsevier, Amsterdam, **2001**; b) T. Ohsuna, B. Slater, F. Gao, J. Yu, Y. Sakamoto, G. Zhu, O. Terasaki, D. E. W. Vaughan, S. Qiu, C. R. Catlow, *Chem. Eur. J.* **2004**, *10*, 5031–5040.
[16] a) C. Minkowski, G. Calzaferri, *Angew. Chem.* **2005**, *117*, 5459–5463; *Angew. Chem. Int. Ed.* **2005**, *44*, 5325–5329; b) K. Lutkouskaya, G. Calzaferri, *J. Phys. Chem. B* **2006**, *110*, 5633–5638.
[17] A. Z. Ruiz, H. Li, G. Calzaferri, *Angew. Chem.* **2006**, *118*, 5408–5413; *Angew. Chem. Int. Ed.* **2006**, *45*, 5282–5287.
[18] A. Khatyr, H. Maas, G. Calzaferri, *J. Org. Chem.* **2002**, *67*, 6705–6710.
[19] a) H. Maas, G. Calzaferri, *Angew. Chem.* **2002**, *114*, 2389–2392; *Angew. Chem. Int. Ed.* **2002**, *41*, 2284–2288; b) G. Calzaferri, US and EU patent WO 02/36490 A1, priority date, **2000**, granted US **2005**, EU **2006**.
[20] a) J. S. Lee, H. Lim, K. Ha, H. Cheong, K. B. Yoon, *Angew. Chem.* **2006**, *118*, 5414–5414; *Angew. Chem. Int. Ed.* **2006**, *45*, 5288–5292; b) K. B. Yoon, *Acc. Chem. Res.* **2007**, *40*, 29–40.
[21] S. Huber, G. Calzaferri, *ChemPhysChem* **2004**, *5*, 239–242.
[22] R. Bonneau, J. Pereyre, *Photochem. Photobiol.* **1975**, *21*, 173–177.
[23] U. Sommer, H. E. A. Kramer, *Photochem. Photobiol.* **1971**, *13*, 387–398.
[24] H. Musso, H.-G. Matthies, H. Krämer, P. Hocks, *Chem. Ber.* **1960**, *93*, 1782–1788.
[25] L. Michaelis, S. Garnick, *J. Am. Chem. Soc.* **1941**, *63*, 1636–1643.
[26] "pH im Innern der Kanäle und Einfluss der Kokationen auf Einbau und Fluoreszenz von Oxonin in Zeolith L": P. Anliker, Diploma Thesis, DCB Universität Bern (Switzerland), **2002**.
[27] H. Musso, C. Rathjen, *Chem. Ber.* **1959**, *92*, 751–753.

[28] "Das organische Farbstoffmolekül Resorufin und dessen Einbau in Zeolith L": D. Brühwiler, Diploma Thesis, DCB Universität Bern (Switzerland), **1996**.
[29] G. Calzaferri, D. Brühwiler, S. Megelski, M. Pfenniger, M. Pauchard, B. Hennessy, H. Maas, A. Devaux, U. Graf, *Solid State Sci.* **2000**, *2*, 421–447.
[30] F. Márquez, C. M. Zicovich-Wilson, A. Corma, E. Palomares, H. García, *J. Phys. Chem. B* **2001**, *105*, 9973–9979.
[31] V. Ramamurthy, D. R. Sanderson, D. F. Eaton, *J. Am. Chem. Soc.* **1993**, *115*, 10438–10439.
[32] D. W. Breck, *Zeolite Molecular Sieves. Structure, Chemistry and Use*, Wiley, New York, **1974**.
[33] M. Pfenniger, G. Calzaferri, *ChemPhysChem* **2000**, *1*, 211–217.
[34] M. M. Yatskou, M. Meyer, S. Huber, M. Pfenniger, G. Calzaferri, *ChemPhysChem* **2003**, *4*, 567–587.
[35] B. Valeur, *Molecular Fluorescence: Principles and Applications*, Wiley-VCH, Weinheim, **2002**.
[36] K. K. Smith, K. J. Kaufmann, D. Huppert, M. Gutman, *Chem. Phys. Lett.* **1979**, *64*, 522–527.
[37] P. Iwa, U. E. Steiner, E. Vogelmann, H. E. A. Kramer, *J. Phys. Chem.* **1982**, *86*, 1277–1285.
[38] H. S. Kim, K. W. Sohn, Y. Jeon, H. Min, D. Kim, K. B. Yoon, *Adv. Mater.* **2007**, *19*, 260–263.
[39] S. J. Hawkes, *J. Chem. Educ.* **1996**, *73*, 516–517.
[40] U. Simon, M. E. Franke in *Host–Guest Systems Based on Nanoporous Crystals*, (Eds.: F. Laeri, F. Schüth, U. Simon, M. Wark), Wiley-VCH, Weinheim, **2003**, pp. 364–378.
[41] G. Calzaferri, R. Giovanoli, I. Kamber, R. Nesper, V. Shklover, *Res. Chem. Intermed.* **1993**, *19*, 31–57.
[42] Y. Komori, S. Hayashi, *Chem. Mater.* **2003**, *15*, 4598–4603.
[43] T. Doussineau, M. Smaïhi, S. Balme, J.-M. Janot, *ChemPhysChem* **2006**, *7*, 583–589.
[44] M. B. J. Roeffaers, B. F. Sels, H. Uji-i, B. Blanpain, P. L'hoëst, P. A. Jacobs, F. C. De Schryver, J. Hofkens, D. E. De Vos, *Angew. Chem.* **2007**, *119*, 1736–1739; *Angew. Chem. Int. Ed.* **2007**, *46*, 1706–1709.
[45] S. Hashimoto, H. R. Moon, K. B. Yoon, *Microporous Mesoporous Mater.* **2007**, *101*, 10–18.
[46] M. N. Chrétien, *Pure Appl. Chem.* **2007**, *79*, 1–20.
[47] D. Brühwiler, N. Gfeller, G. Calzaferri, *J. Phys. Chem. B* **1998**, *102*, 2923–2929.
[48] V. Ramamurthy, J. V. Caspar, D. R. Corbin, D. F. Eaton, *J. Photochem. Photobiol. A* **1989**, *50*, 157–161.
[49] M. J. S. Dewar, E. G. Zoebisch, E. F. Healy, J. J. P. Stewart, *J. Am. Chem. Soc.* **1985**, *107*, 3902–3909.
[50] M. C. Zerner, G. H. Loew, R. F. Kirchner, U. T. Mueller-Westerhoff, *J. Am. Chem. Soc.* **1980**, *102*, 589–599.
[51] A. Z. Ruiz, D. Brühwiler, T. Ban, G. Calzaferri, *Monatsh. Chem.* **2005**, *136*, 77–89.
[52] H. Eichler, *J. Prakt. Chem.* **1934**, *139*, 113–114.
[53] W. Müller, *Justus Liebigs Ann. Chem.* **1974**, 334–335.
[54] H. Maas, A. Khatyr, G. Calzaferri, *Microporous Mesoporous Mater.* **2003**, *65*, 233–242.
[55] a) G. Calzaferri, R. Rytz, M. Brändle, D. Brühwiler, S. Glaus, ICON-EDiT, Extended-Hückel Molecular Orbital and Electronic Dipole-induced Transition Calculations; available at http://www.dcb.unibe.ch/groups/calzaferri/start.html, update **2000**; b) G. Calzaferri, L. Forss, I. Kamber, *J. Phys. Chem.* **1989**, *93*, 5366–5371; c) R. Hoffmann, *J. Chem. Phys.* **1963**, *39*, 1397–1400.
[56] HyperChem, Hypercube Inc., 1115 NW 4th Street, Gainesville, Florida 32601, USA, **2003**.

Received: April 12, 2007
Revised: June 21, 2007
Published online: September 20, 2007

